Structure of the Catalytic Domain of Human Protein Kinase C β II Complexed with a Bisindolylmaleimide Inhibitor‡

Neil Grodsky,§,|| Ying Li,§,⊥ Djamal Bouzida,|| Robert Love,|| Jordan Jensen,⊥ Beverly Nodes,⊥ Jim Nonomiya,⊥ and Stephan Grant*,⊥

Departments of Biochemical Pharmacology and Structural and Computational Biology and Design, Pfizer Global Research and Development, Pfizer La Jolla Laboratories, 10777 Science Center Drive, San Diego, California 92121

Received June 6, 2006; Revised Manuscript Received August 14, 2006

ABSTRACT: The conventional protein kinase C isoform, PKCβII, is a signaling kinase activated during the hyperglycemic state and has been associated with the development of microvascular abnormalities associated with diabetes. PKCβII, therefore, has been identified as a therapeutic target where inhibitors of its kinase activity are being pursued for treatment of microvascular-related diabetic complications. In this report, we describe the crystal structure of the catalytic domain of PKCβII complexed with an inhibitor at 2.6 Å resolution. The kinase domain of PKCβII was cleaved and purified from full-length PKCβII expressed in baculovirus-infected insect cells. The overall kinase domain structure follows the classical bilobal fold and is in its fully activated conformation with three well-defined phosphorylated residues: Thr-500, Thr-641, and Ser-660. Different from the crystal structures of nonconventional PKC isoforms, the C-terminus of the PKCβII catalytic domain is almost fully ordered and features a novel α helix in the turn motif. An ATP-competitive inhibitor, 2-methyl-1*H*-indol-3-yl-BIM-1, was crystallized with the PKCβII catalytic domain as a dimer of two enzyme−inhibitor complexes. The bound inhibitor adopts a nonplanar conformation in the ATP-binding site, with the kinase domain taking on an intermediate, open conformation. This PKCβII−inhibitor complex represents the first structural description of any conventional PKC kinase domain. Given the pathogenic role of PKCβII in the development of diabetic complications, this structure can serve as a template for the rational design of inhibitors as potential therapeutic agents.

The protein kinase C (PKC) family belongs to the AGC superfamily of serine/threonine kinases. The PKC enzymes are involved in signal transduction events responding to specific hormonal, neuronal, and growth factor stimuli (*1*, *2*). The PKC family comprises more than 10 isozymes grouped into three classes based on their structure and cofactor regulation (*3*−*7*). The conventional PKCs (α, γ, and the alternatively spliced βI and βII) require diacylglycerol (DAG), phosphatidylserine (PS), and calcium for activation. The novel PKCs (δ, ϵ, η/λ, θ) are activated by DAG and PS but are insensitive to calcium. The atypical PKCs (ζ and ι/λ) only require PS but neither DAG nor calcium for full activity.

PKCβII has been implicated as a key player in the pathogenesis of diabetic microvascular complications such as retinopathy, nephropathy, and neuropathy (*8*). Among the PKC isoforms, PKCβII is a predominant isozyme activated in vascular tissues during hyperglycemia, the underlying factor for diabetic vascular abnormalities (*9*−*11*). The activation of PKCβII may increase retinal endothelial permeability, increase basement membrane protein synthesis, and stimulate angiogenesis (*12*−*14*). The role of PKCβII was assessed in a model of ischemia-induced retinopathy using transgenic, PKCβII-overexpressing animals (*15*). Ischemia-induced retinopathy caused neovascularization of the retina in control mice. This response was markedly increased in the transgenic, PKCβII-overexpressing animals. In contrast, mice with a targeted disruption of the PKCβ gene (knockout) showed a markedly diminished neovascularization response to the same ischemic insult (*15*). Ruboxistaurin (LY333531 mesylate), a specific PKCβII inhibitor, has been tested in clinical studies for diabetic retinopathy, neuropathy, and nephropathy. Treating diabetic animals with ruboxistaurin ameliorated retinopathy associated with pathological changes such as reduced retinal blood flow, increased retinal mean circulation time, and diabetes-induced retinal vascular permeability and leakage (*16*, *17*). The results from these preclinical studies and recent clinical trials for diabetic retinopathy (*18*), diabetic macular edema (*19*), and diabetic nephropathy (*20*) with ruboxistaurin lend encouraging support for the development and use of PKCβII inhibitors as pharmaceutical agents for the treatment of diabetic microvascular complications.

PKCβII, like other members of the PKC family, has a conserved N-terminal regulatory region and a C-terminal catalytic region or kinase domain (Figure 1A). A proteolytically labile hinge sequence connects the regulatory domain to the catalytic domain (*21*). The regulatory domain consists of several well-defined structural features, which include

‡ Atomic coordinates have been deposited in the Protein Data Bank with access code 2I0E.

* Corresponding author. Phone: (858) 526-4732. Fax: (858) 526-4496. E-mail: stephan.grant@pfizer.com.

§ These two authors made equal contributions to this work.

|| Department of Structural and Computational Biology and Design.

⊥ Department of Biochemical Pharmacology.

10.1021/bi061128h CCC: $33.50
Published on Web 11/03/2006

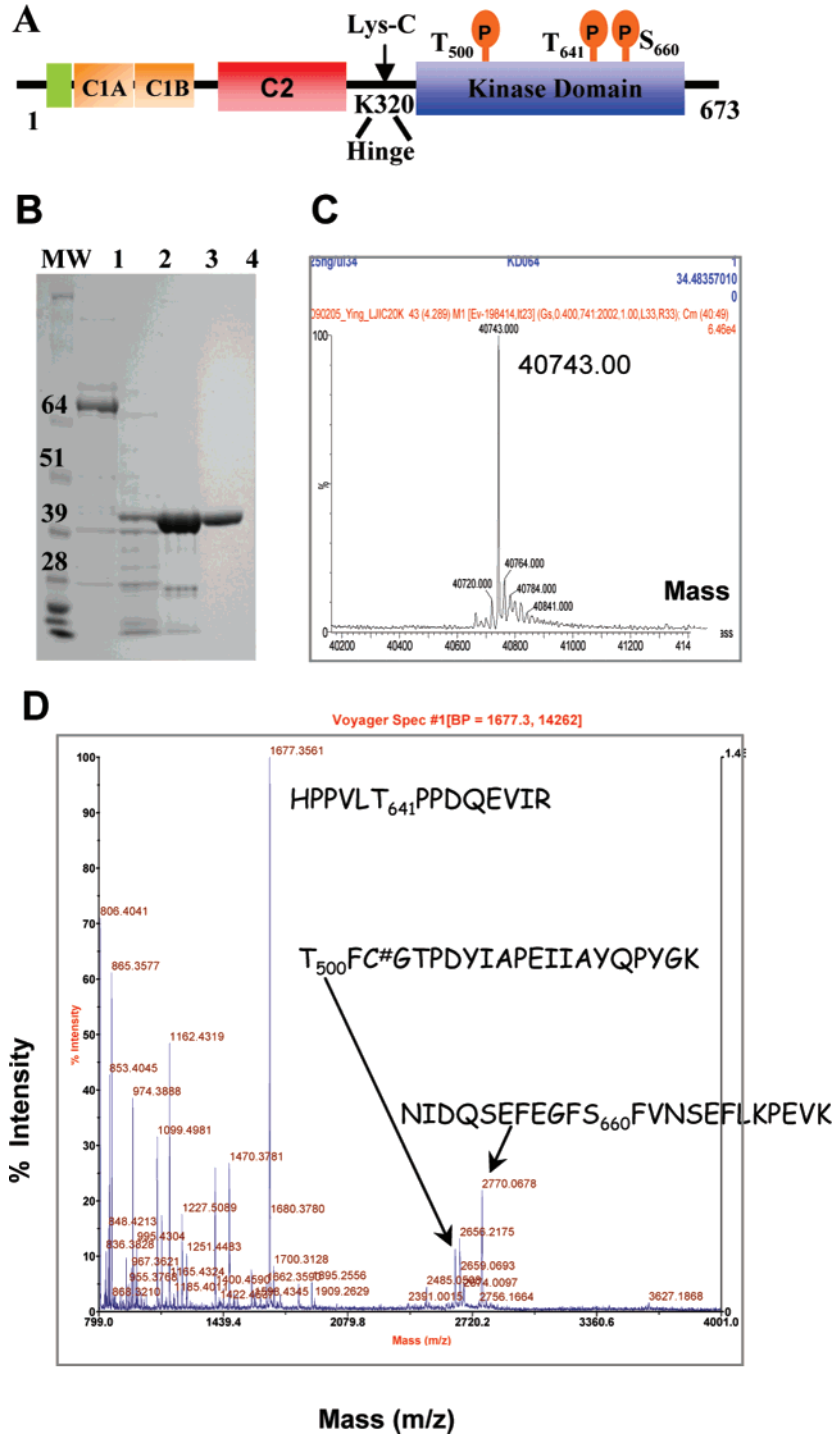

FIGURE 1: Purification and characterization of the PKCβII catalytic domain. (A) Schematic representation of the regulatory and kinase domain structure of conventional PKC showing an autoinhibitory pseudosubstrate sequence (colored green) N-terminal to the C1A and C1B domains (colored orange), the C2 domain (colored red), and a conserved kinase core (colored blue) with the three phosphorylation sites (Thr-500, Thr-641, and Ser-660) indicated. The hinge region is proteolytically labile where the endoproteinase Lys-C cleaves PKCβII at the carboxy terminus of Lys-320. (B) The PKCβII catalytic domain was obtained by Lys-C digestion (lane 2) of the full-length PKCβII (lane 1). The protein was further purified on MonoQ (lane 3) and HiLoad Superdex 200 columns (lane 4). (C) The intact mass of the PKCβII catalytic domain was 40743.0 Da. (D) Mass spectra of tryptic digests identified three phosphorylation sites: (i) HPPVLT$_{641}$-PPDQEVIR at *m*/*z* 1677.4 indicates that Thr-641 is the phosphorylation site; (ii) NIDQSEFEGFS$_{660}$FVNSEFLKPEVK at *m*/*z* 2770.1 indicates that this peptide contains one phosphate; and (iii) T$_{500}$FC$^{\#}$GTPDYIAPEIIAYQPYGK at *m*/*z* 2485.1 indicates that this peptide contains one phosphate (the cysteine carbamidomethylated by iodoacetamide is followed by #).

binding sites for lipids and cofactors that are involved in the translocation and activation of PKC. Within the regulatory region, the C1 domain contains two cysteine-rich zinc finger motifs that bind DAG, PS, and phorbol esters (*22*). The C2 domain is involved in calcium-dependent membrane binding (*23*). The catalytic or kinase domain requires phosphorylation at three sites for full activation (*24*, *25*): phosphorylation of threonine 500 (Thr-500) in the activation loop by the upstream kinase PDK-1 is a prerequisite for the maturation of the enzyme (*26*), which subsequently leads to autophosphorylation at threonine 641 (Thr-641) in the turn motif and serine 660 (Ser-660) in the hydrophobic motif (*27*).

Among the PKC family, structural information is available for the C1 domain of PKCδ (residues 231−280) (*28*) and the C2 domains of conventional PKCs such as PKCα (residues 155−293) (*29*), PKCβ (*30*), and PKCδ (residues 1−123) (*31*). Structural information has also recently become available for the kinase domains of the novel PKC isoform, PKCθ bound with staurosporine (*32*), and of the atypical PKC isoform, PKCι in complex with BIM-1 (*33*).

Despite their essential functions and importance in diabetes research, protein crystal structures of the kinase domains of conventional PKCs, notably PKCβII, have remained refractory to elucidation. Here, we present the first structural determination of the catalytic, kinase domain of PKCβII with a bound potent, ATP-competitive inhibitor. An evaluation of the structural features of this kinase is provided in comparison to related AGC family members. In addition, we investigated the potential active site interactions of clinical candidate ruboxistaurin by modeling the compound into the ATP-binding site. This PKCβII kinase domain structure provides an essential tool for a structure-based drug design approach to the development of novel inhibitors for this important signaling enzyme.

MATERIALS AND METHODS

Reagents. The following chemical reagents were purchased from Sigma (St. Louis, MO): ADA,[1] ATP, $CaCl_2$, DMSO, DTT, HEPES, $MgCl_2$, NADH, phosphoenol pyruvate (PEP), phosphatidylserine (PS), Lys-C, pyruvate kinase, and lactate dehydrogenase. Sodium acetate was purchased from Fisher Scientific (Pittsburgh, PA). Phorbol myristate acetate (PMA) and 3-(1-(3-(dimethylamino)propyl)-1*H*-indol-3-yl)-4-(1*H*-indol-3-yl)-1*H*-pyrrole-2,5-dione (BIM-1) were obtained from Calbiochem (San Diego, CA). Diacylglycerol (1,2-dioleoyl-*sn*-glycerol, DAG) was obtained from Avanti Polar Lipids (Alabaster, AL). Human recombinant, full-length PKC isoforms (PKC-alpha, beta-I, beta-II, gamma, delta, theta, epsilon, eta, zeta) were obtained from Calbiochem and PKC-iota was from Upstate USA (Charlottesville, VA). PKC peptide substrate (RFARKGSLRQKNV) was purchased from American Peptide Co. (Sunnyvale, CA). The 2B9 phosphoserine antibody was purchased from MBL International (Woburn, MA). PefablocSC was from Pentapharm (Basel, Switzerland). The bisindolylmaleimide analogue of BIM-1, 3-(1-(3-(dimethylamino)propyl)-2-methyl-1*H*-indol-3-yl)-4-(2-methyl-1*H*-indol-3-yl)-1*H*-pyrrole-2,5-dione (2-methyl-1*H*-indol-3-yl-BIM-1) was from the Pfizer chemical collection.

Expression and Purification of the PKCβII Kinase Domain. The human PKCβII catalytic or kinase domain (residues 321−673) was obtained by proteolytic cleavage of the full-length PKCβII expressed in recombinant baculovirus-infected SF21 cells. The DNA for the N-terminal hexahistidine-tagged full-length PKCβII (residues 2−673) was cloned into pAcSG2 (BD Bioscience, San Diego, CA) using the *Xho*I and *Stu*I restriction sites. The recombinant viruses were prepared using standard procedures provided by the manufacturer (BD Bioscience).

For expression, SF21 cells at 2×10^6 cells/mL were infected with 0.2% (v/v) virus and then harvested at 72 h postinfection. The cell pellet was resuspended in lysis buffer (20 mM HEPES, pH 7.5, 10 mM β-mercaptoethanol, 0.3 M NaCl, 5 mM sodium pyrophosphate, 10 mM β-glycerol phosphate, 50 mM sodium fluoride, 10 mM imidazole, 1 mM PefablocSC, 0.5% Triton X-100, and 10% glycerol), dounce-homogenized, and lysed in a microfluidizer. The lysate was centrifuged at 10000 rpm for 45 min, and the cell-free lysate was then incubated with Ni-NTA−agarose beads (Qiagen) for 2 h at 4 °C. The nickel beads were collected by centrifugation at 3000 rpm for 5 min, washed with buffer A (20 mM HEPES, pH 7.5, 10 mM β-mercaptoethanol, 0.3 M NaCl, 20 mM imidazole, 0.1% Triton X-100, and 10% glycerol), and then eluted with buffer B (20 mM HEPES, pH 7.5, 10 mM β-mercaptoethanol, 0.3 M NaCl, 0.3 M imidazole, 0.1% Triton X-100, and 10% glycerol). The resultant *N*-His-tagged, full-length PKCβII solution was exchanged into a protease digestion buffer (20 mM HEPES, pH 7.5, 10 mM β-mercaptoethanol, 0.3 M NaCl, 0.05% Triton X-100, and 10% glycerol) via overnight dialysis at 4 °C.

The catalytic domain of PKCβII was obtained by digestion of the full-length protein with the protease Lys-C and then loaded on a Mono Q HR 10/100GL column (GE Healthcare). The column was washed with Mono Q buffer (20 mM HEPES, pH 7.5, 0.15 M NaCl, 5 mM DTT, and 10% glycerol) before being resolved by the application of a linear gradient from 0.15 to 0.4 M NaCl. Fractions containing the catalytic domain were pooled, concentrated, and further purified on a HiLoad Superdex 200 (16/60) column (GE Healthcare) equilibrated in S200 buffer (20 mM HEPES, pH 7.5, 0.15 M NaCl, 5 mM DTT, and 5% glycerol). The purified PKCβII kinase domain was concentrated to 8 mg/mL and stored frozen at −80 °C.

Mass Spectrometric Analysis. Intact protein mass spectra were recorded on a Micromass Q-ToF Micro mass spectrometer (Waters, Beverly, MA), operated in ToF-only mode. Typically, a 5 μg sample of the intact PKCβII kinase domain protein (in 20 mM HEPES, pH 7.5, 0.15 M NaCl, 5 mM DTT, and 5% glycerol) was prepared for analysis by offline desalting using C4 or C18 ZipTips (Millipore, Billerica, MA) according to the manufacturer's instructions. Following desalting, the ZipTip-bound protein was eluted in 5 μL of 50% acetonitrile/1% formic acid aqueous solution. Approximately 1.5 μL of the desalted protein solution was sprayed directly into the mass spectrometer orifice using a nanoelectrospray capillary (Proxeon Biosystems, Odense, Denmark) for a 3 min acquisition period (capillary voltage = 700 V, sample cone voltage = 35 V, extraction cone voltage = 0.5 V). The raw mass spectra were deconvoluted for average molecular mass using MaxEnt 1 software (Waters, Beverly, MA) with a resolution setting of 1.0 Da/channel and peak width at half-height setting of 1.5 Da.

The mass spectra of tryptic digests were recorded on a Voyager DE-PRO MALDI mass spectrometer (Applied Biosystems, Foster City, CA) equipped with a 337 nm nitrogen laser and an Acqiris 2 GHz digitizer. Typically, a 5 μg sample of the PKCβII catalytic subunit was electrophoretically separated on a 4−12% SDS−NuPAGE gel (Invitrogen, Carlsbad, CA) and stained with SYPRO Orange (Invitrogen). The bands of interest were excised, washed with

[1] Abbreviations: ADA, acetamidoiminodiacetic acid; DMSO, dimethyl sulfoxide; DTT, dithiothreitol; Ni-NTA, nickel nitrilotriacetic acid; SDS−PAGE, sodium dodecyl sulfate−polyacrylamide gel electrophoresis; MALDI, matrix-assisted laser desorption/ionization.

50% methanol, and equilibrated with 50% acetonitrile/25 mM ammonium bicarbonate. The equilibrated gel slices were dried by vacuum centrifugation and then resuspended in 10 μL of 0.01 mg/mL modified porcine trypsin (Promega, Madison, WI) in 25 mM ammonium bicarbonate; the digests were incubated for at least 2 h at 37 °C. For MALDI analysis, 0.5 μL of the tryptic digest solution was spotted on a MALDI sample plate, followed by 0.5 μL of a 10 mg/mL solution of 2,5-dihydroxybenzoic acid in 50% acetonitrile/0.1% TFA aqueous solution; sample drops were allowed to air-dry. Mass spectra were acquired in reflectron mode, typically accumulating 100 shots per spectrum (laser intensity = 1600, acceleration voltage = 20 kV, grid voltage = 74 V, guide wire = 75 ns).

Exact phosphorylation sites were determined by MS/MS sequencing of the tryptic digests on a Micromass Q-ToF Micro mass spectrometer. Samples were prepared for analysis by mixing 1 μL of tryptic digest with 1 μL of 98% acetonitrile/2% formic acid. Approximately 1.5 μL of the resulting mixture was sprayed directly into the mass spectrometer orifice using a nanoelectrospray capillary. MS/MS spectra of phosphopeptides were recorded for an acquisition time of 3−60 min, depending on the abundance and length of the sequencing target (capillary voltage = 700 V, sample cone voltage = 35 V, extraction cone voltage = 0.5 V, collision energy = 25−55 eV, depending on the length of the peptide). MS/MS spectra were manually interpreted to locate phosphorylated amino acids.

Enzyme Assays. The dose-dependent inhibition (IC_{50}) of PKC isoforms was evaluated by a fluorescence polarization-based, activity assay as described previously (*34*). The assay utilized a specific, phosphoserine antibody (2B9) and a fluorescent TAMRA-labeled peptide tracer. PKC activity was detected by measuring the fluorescence polarization ratio between the free and antibody-bound fluorescent tracer as it was displaced from the antibody by the PKC phosphopeptide reaction product. The assay conditions were optimized for each PKC isoform with the following concentration ranges for protein (7.5−240 pM), ATP (10 μM to 0.1 mM), and peptide substrate (0.5−4.5 μM). The PS concentration was 1.0 μg/mL and the DAG concentration was 0.2 μg/mL. Dose−response curves for inhibitors were determined in duplicate. The PKC reactions were incubated at room temperature for 30 min and stopped by addition of a quench solution containing 15 mM EDTA, 3.1 nM tracer, and 3.0 nM antibody. The fluorescence polarization values were measured with a LJL Analyst microtiter plate reader (excitation = 535 nm, emission = 580 nm).

Kinetic and mechanistic studies of PKCβII and PKCα utilized a pyruvate kinase−lactate dehydrogenase coupled, continuous spectrophotometric assay where the phosphorylation of a PKC peptide substrate (RFARKGSLRQKNV) was coupled to the oxidation of NADH and the corresponding change in absorbance intensity was measured at 340 nm (*35*, *36*). A typical assay was carried out on a 96-well, clear microtiter plate in a Molecular Devices spectrophotometer for 20 min at 30 °C in 0.1 mL of assay buffer containing 50 mM HEPES, pH 7.4, 1−5 nM PKC, 30 units of pyruvate kinase, 25 units of lactate dehydrogenase, 0.15 mM peptide, 0.1 mM ATP, 1 mM DTT, 4 mM PEP, 8 mM $MgCl_2$, 0.3 mM NADH, 60 μM $CaCl_2$, 10 μg/mL PS, 50 ng/mL PMA, and 7.5% DMSO. Stock solutions of PS and PMA were sonicated for 30 s just prior to addition to assay buffer, and assays were initiated by the addition of ATP. Steady-state kinetic parameters for the bi-bi kinase reaction were determined at saturating phosphoacceptor peptide substrate concentration (0.15 mM) by fitting initial velocity data to the Michaelis−Menten equation:

$$v = V_{max}[S]/(K_M + [S])$$

where v is the measured initial velocity, V_{max} is the maximal enzyme velocity, [S] is the ATP substrate concentration, and K_M is the Michealis constant for ATP. Enzyme turnover values (k_{cat}) were calculated according to $k_{cat} = V_{max}[E]$, where [E] is the total enzyme concentration. Enzyme inhibition constants (apparent K_i values) were determined by fitting initial velocities at variable inhibitor concentrations to a model for ATP-competitive inhibition based on the Morrison equation (*37*).

Crystallization and Structure Determination. The PKCβII catalytic domain (residues 321−673) was concentrated to approximately 8 mg/mL for crystallization. Initial small red rods were obtained at 13 °C from hanging drops containing 1 μL of protein−compound solution (∼1:4 molar ratio) and 1 μL of precipitating solution (0.1 M ADA, pH 6.5, and 2.0 M sodium acetate). Larger crystals were obtained using larger drops (2−4 μL) and a precipitating solution of 0.1 M ADA, pH 6.0−7.0, and 1.7−2.3 M sodium acetate. Crystals were mounted in Hampton loops, dipped in a cryoprotectant of 0.1 M ADA, pH 6.5, and 2.5 M sodium acetate, and either flash frozen in liquid nitrogen or frozen in the cryostream. Initial diffraction data were obtained using a CCD detector (MAR Research, Hamburg, Germany) installed on a Rigaku-MSC FR-D rotating anode X-ray generator (Rigaku/MSC, Inc., The Woodlands, TX) equipped with Osmic mirrors (Osmic, Inc., Troy, MI) and an X-stream cryogenic system (Rigaku-MSC, Inc.), yielding 3.2 Å resolution data. All data were processed using HKL2000 software (HKL Research, Charlottesville, VA) (*38*). The space group was identified as $P2_12_12$ with unit cell dimensions of approximately a = 93 Å, b = 131 Å, and c = 84 Å. A subsequent data set was collected to a resolution of 2.6 Å at the Advanced Light Source, Beamline 5.0.1 (Berkeley, CA), using a Quantum-210 CCD detector (Area Detector Systems).

The structure was determined by molecular replacement with the program AMoRe (*39*) using an in-house homology model of PKCβII kinase domain based on the crystal structure of AKT-1 (unpublished data) as the search model, giving two molecules (monomers A and B) in the asymmetric unit. Initial refinement was performed using CNX (Accelrys, Inc., San Diego, CA) and later refinement using REFMAC5 (*40*). X-FIT (*41*) was used for model building. The final refined model includes residues 339−624 and 627−669 for monomer A and residues 339−620 and 651−669 in monomer B, along with 115 water molecules and two inhibitors. Ramachandran plot analysis using PROCHECK (*42*) showed 99.1% of residues falling into most favored or additionally allowed regions, with 0.9% (five residues) generously allowed, and 0% disallowed. Results from data collection and refinement statistics are shown in Table 1. Structural figures were generated using PyMOL (*43*).

In the crystal lattice of PKCβII, a copy of molecule A related by crystallographic symmetry, denoted here A′, is

Table 1: Data Collection and Refinement Statistics

data collection[a]	
space group	$P2_12_12$
unit cell (*a*, *b*, *c* in Å)	93.1, 131.4, 83.8
resolution range (Å)	50.0−2.6
observations	131998
unique reflections	32375
completeness (%)	99.7 (100)
$\langle I/\sigma_I \rangle$	28.4 (3.0)
R_{sym} (%)[b]	4.9 (48.4)
structure refinement	
resolution range (Å)	30.0−2.6
reflections used	31651
R-factor, R_{free} (%)[c]	23.5, 28.9
no. of protein + inhibitor atoms	5169
no. of water molecules	115
average *B* (Å^2)	54.6
rms deviations from ideal values	
bond lengths (Å)	0.010
bond angles (deg)	1.330

[a] Values in parentheses refer to the highest resolution shell (2.69−2.60 Å). [b] $R_{sym} = \sum|I - \langle I\rangle|/\sum I$, where *I* is measured intensity for reflections with indices *hkl*. [c] *R*-factor = $100(\sum|F_o| - |F_c|/\sum|F_o|)$; R_{free} = free *R*-factor based on random 5% of all data.

positioned such that the first 10 residues of the C-terminus from each copy are in close mutual proximity (Figure 5A). As a result, residue 627′ of A′ is near residue 624 of A (∼10 Å). Thus it is conceivable that 624A could be connected to 627A′ such that helix 628A′−636A′ becomes part of molecule A. However, in that case the remaining C-terminus of molecule A′ would exchange with neighboring molecule A. In support of the 624A−627A trace and relatively compact model presented here, another cocrystal structure of PKC*β*II involving a different inhibitor and different crystal packing (with only one molecule per asymmetric unit) was recently determined in our laboratory (at lower resolution; data not shown) and featured a similar trace of the C-terminus.

Homology and Molecular Modeling. To generate the homology model of the PKC*β*II kinase domain, we performed a sequence alignment analysis to select the closest kinase domain surrogate crystal structure to generate the model, using Vector NTI software (Informax, Inc.). The kinase domains and active site residues for five kinases, namely, PKCα, PKC*β*II, PKC*θ*, PKAα, and AKT1, were compared using this multiple alignment technique. The PKC isoforms were found to be much more similar to AKT1 than PKAα (∼50% vs 40% identity of the kinase domain, and 10 out of 17 nonconserved active site residues were found to be exactly the same between PKC*β*II and AKT1, whereas only 6 out of 17 residues were identical between PKC*β*II and PKAα). This analysis therefore indicated that an AKT1 structure was more suitable as a surrogate model for PKC homology modeling. The homology model was generated using the MODELER module within the InsightII software (Accelrys, Inc., InsightII 2005). Although the C-terminal tail modeling proved to be challenging, special care was taken to refine this region of the kinase by defining and aligning specific basic residues (arginine and lysine) that were more likely to ligate the charged phosphates from the two known PKC kinase domain phosphorylation sites.

To model the ATP-competitive inhibitor, ruboxistaurin, within the PKC*β*II kinase domain structure, we used the AGDOCK software (*44*, *45*). This method employed a simplistic, short-ranged potential and an evolutionary programming strategy to evolve the docking solutions. The selected bond lengths and angles were those of the *S*-enantiomer of this compound as was cocrystallized in PDK1 (*46*). The macrocycle was kept rigid during the docking but could translate and rotate freely within the active site. The modeling was performed in replicate experiments, each containing 50 docking conformations. Reproducible and high consensus docks were obtained from the replicate experiments.

RESULTS AND DISCUSSION

*Expression and Purification of the PKC*β*II Kinase Domain.* Initial attempts to express the PKC*β*II catalytic (or kinase) domain in *Escherichia coli* were unsuccessful. The protein expressed in *E. coli* was in the insoluble fraction (data not shown), likely due to lack of phosphorylation and/or improper folding. Further attempts to express the PKC*β*II catalytic domain in insect cells resulted in very low yield of partially active protein (data not shown). However, the full-length PKC*β*II protein was successfully expressed in insect cells with reasonable yield. Although a majority of the insect cell-expressed full-length protein was insoluble (data not shown), active and stable full-length PKC*β*II was purified from the soluble fraction. Taking advantage of the fact that the hinge region between the N-terminal regulatory domain and the C-terminal kinase domain is proteolytically labile (*21*), the active PKC*β*II catalytic domain (residues 321−673) used for crystallization was generated by protease digestion of the full-length protein. Complete cleavage of the full-length protein was obtained by two methods. In the first, Lys-C was utilized to take advantage of an endogenous Lys-C site existing in the hinge region (Figure 1B). N-Terminal sequence analysis confirmed that the catalytic domain obtained by Lys-C treatment started at Thr-321 (data not shown). Alternatively, a PreScission protease recognition site (LEVLFQGP) was inserted by mutagenesis into the hinge region of the full-length protein, and the PKC*β*II kinase domain was then obtained by incubation with the PreScission protease (data not shown). Q-ToF mass spectroscopic analysis suggested that >95% of the protein was in a single peak of 40743.0 Da (Figure 1C), indicating that the protein was sufficiently pure for crystallization trials. The mass of 40743 Da agreed well with the expected kinase domain mass for 353 residues with three phosphates. MALDI mass spectroscopic analysis of the tryptic digest identified the positions of the phosphorylation sites at Thr-641 and within two peptides containing Thr-500 or Ser-660, respectively (Figure 1D). MS/MS sequencing was further performed and definitively identified the exact phosphorylation sites at Thr-500, Thr-641, and Ser-660 (data not shown). These three phosphorylated residues were all well-defined in the resulting protein cocrystal structure of the PKC*β*II kinase domain.

*Kinetic Characterization of the PKC*β*II Kinase Domain*. The specific activity of *N*-His-tagged full-length PKC*β*II was found to be similar to human, recombinant PKC*β*II obtained from a commercial vendor. The specific activity of the kinase domain obtained by proteolytic processing of the full-length PKC*β*II was identical to the full-length protein containing the regulatory domain. Kinetic parameters were determined for the full-length PKC*β*II and kinase domain and showed similar values (Table 2) for turnover of a peptide substrate

Table 2: Kinetic Parameters for Full-Length PKCβII and Its Kinase Domain

PKCβII	k_{cat}, min^{-1}	ATP K_M, μM
full length	550 ± 15	31 ± 3
kinase domain	557 ± 6	34 ± 2

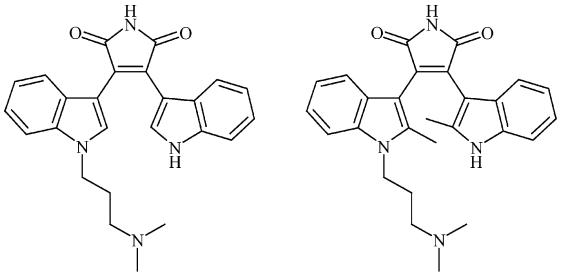

FIGURE 2: Structures of BIM-1 and 2-methyl-1*H*-indol-3-yl-BIM-1.

Table 3: IC_{50} Values (nM) for Inhibition of PKC Isoforms

PKC isoform	BIM-1	2-methyl-BIM-1	PKC isoform	BIM-1	2-methyl-BIM-1
PKCα	3.5	292	PKCθ	2.7	264
PKCβI	2.2	65	PKCϵ	3.1	176
PKCβII	0.6	17	PKCη	9.2	>500
PKCγ	2.3	95	PKCι	>250	>1000
PKCδ	8.2	168	PKCζ	>250	>1000

(k_{cat}, min^{-1}) and affinity for the ATP cofactor (K_M).

The lipid requirement for full activity was also evaluated for the *N*-His-tagged full-length PKCβII and kinase domain (data not shown). As expected, the full-length PKCβII required addition of both PS and DAG for full activity. In contrast, the activity of the kinase domain was independent of the presence of lipids (PS and DAG), demonstrating equivalent specific activity with omission of lipids from the assay buffer.

Inhibition by Bisindolylmaleimides. The bisindolylmaleimides, which are derived from the potent nonselective inhibitor staurosporine, are well-known inhibitors of PKC (*47*). Both BIM-1 and 2-methyl-1*H*-indol-3-yl-BIM-1 (Figure 2) were potent inhibitors of PKCβII, with broad activity against other PKC isoforms. Table 3 shows the IC_{50} values determined for these two inhibitors against various PKC isoforms. BIM-1 was a potent inhibitor against the conventional (PKCα, PKCβI, PKCβII, and PKCγ) and novel (PKCδ, PKCθ, PKCϵ, and PKCη) PKC isoforms but was not active against the atypical PKC isoforms (PKCζ and PKCι). The 2-methyl-1*H*-indol-3-yl-BIM-1 was less potent but broadly active against the panel of PKC isoforms. Yet, compared to BIM-1, the 2-methyl-1*H*-indol-3-yl-BIM-1 compound was more selective toward PKCβII than PKCα and less inhibitory of PKCη.

The mechanism of inhibition of this series of PKC inhibitors has been shown previously to be competitive toward ATP (*47*). This was further confirmed by the recent PKA cocrystal structure with BIM-2 (*48*) where the bound inhibitor was found within the ATP-binding site. For PKCβII and the closely related PKCα, K_i values were determined for these two bisindolylmaleimide inhibitors. There was little selectivity observed for the potency of BIM-1 between PKCβII and PKCα, with K_i values of 0.4 and 5 nM, respectively. However, 2-methyl-1*H*-indol-3-yl-BIM-1 was much more selective (100×) toward PKCβII (K_i = 2 nM) than PKCα (K_i = 216 nM). The potency and selectivity profiles of these inhibitors prompted the screening of the PKCβII kinase domain for cocrystals.

Overall Structure of the PKCβII Kinase Domain. The AGC family of kinases such as PKA, PKB (AKT), and PKC isoforms shares significant sequence homology. PKC isoforms have greater than 60% sequence identity, including three conserved phosphorylation sites (Figure 3). The catalytic domain of PKCβII is folded into the classical bilobal fold (*49*) as seen with other kinases including other PKC subfamily members (Figure 4A). The N-terminal lobe of the PKCβII kinase domain (residues 339−421) consists of a five-stranded β sheet (β1−β5) and two α helices (αB, αC). The C-terminal lobe (residues 426−620) is comprised of eight α helices. The N- and C-terminal lobes are connected by a linker region defined by residues 422−425. These features are present in both copies of the crystal's dimer (i.e., asymmetric unit), denoted monomer A or B.

Key catalytic residues Lys-371, Asp-466, Asp-484, and Asn-471 are invariant among all protein kinases, and within the PKCβII kinase domain these residues have orientations expected for a fully phosphorylated, active kinase. The catalytic loop emanates from the base of the catalytic site and contains the conserved Asp-466, which interacts with the nucleophilic hydroxyl side chain of the substrate, and Asn-471 and serves to stabilize the orientation of Asp-466. As expected, Asn-471 and Asp-484 form part of the Asp-Phe-Gly (DFG) motif at the base of the activation loop, as required for the binding of two divalent cations involved in nucleotide recognition. Lys-371 forms an ion pair with Glu-390 from helix αC, properly aligning helix αC for substrate binding and catalysis (*49*).

All PKC isoforms have three conserved phosphorylation sites that are required for maturation and full activity. In the PKCβII kinase structure, the activation loop and C-terminal hydrophobic motifs of both molecules A and B are phosphorylated at Thr-500 and Ser-660, respectively. Thr-641, in the turn motif, is phosphorylated in molecule A, but that region is disordered in molecule B. The activation loop (residues 484−511) is well ordered and in a fixed, extended conformation as expected when phosphorylated, with hydrogen bonding of the phosphate of pThr-500 to conserved Arg-465, Lys-489, and neighboring Thr-498.

C-Terminus of PKCβII. The C-terminal segment (residues 621−673) of PKCβII, which wraps around the N-lobe, contains a "turn" (residues 624−650) that is conserved among PKC subfamily members, as well as a conserved hydrophobic motif [FxxF(S/T)F/Y] comprised of residues 656−661. The C-terminus is almost fully resolved in molecule A of the crystal's dimer, although there remains ambiguity (weak electron density) in the connectivity between residues 624 and 627 of the turn motif, and the last four residues are disordered (670−673). Most of the C-terminus of monomer B is disordered except for residues 655−665. The hydrophobic motif is found adjacent to a relatively lipophilic groove on the N-lobe in a similar fashion to that reported for other AGC family members such as PKCθ (*32*) and PKA (*48*).

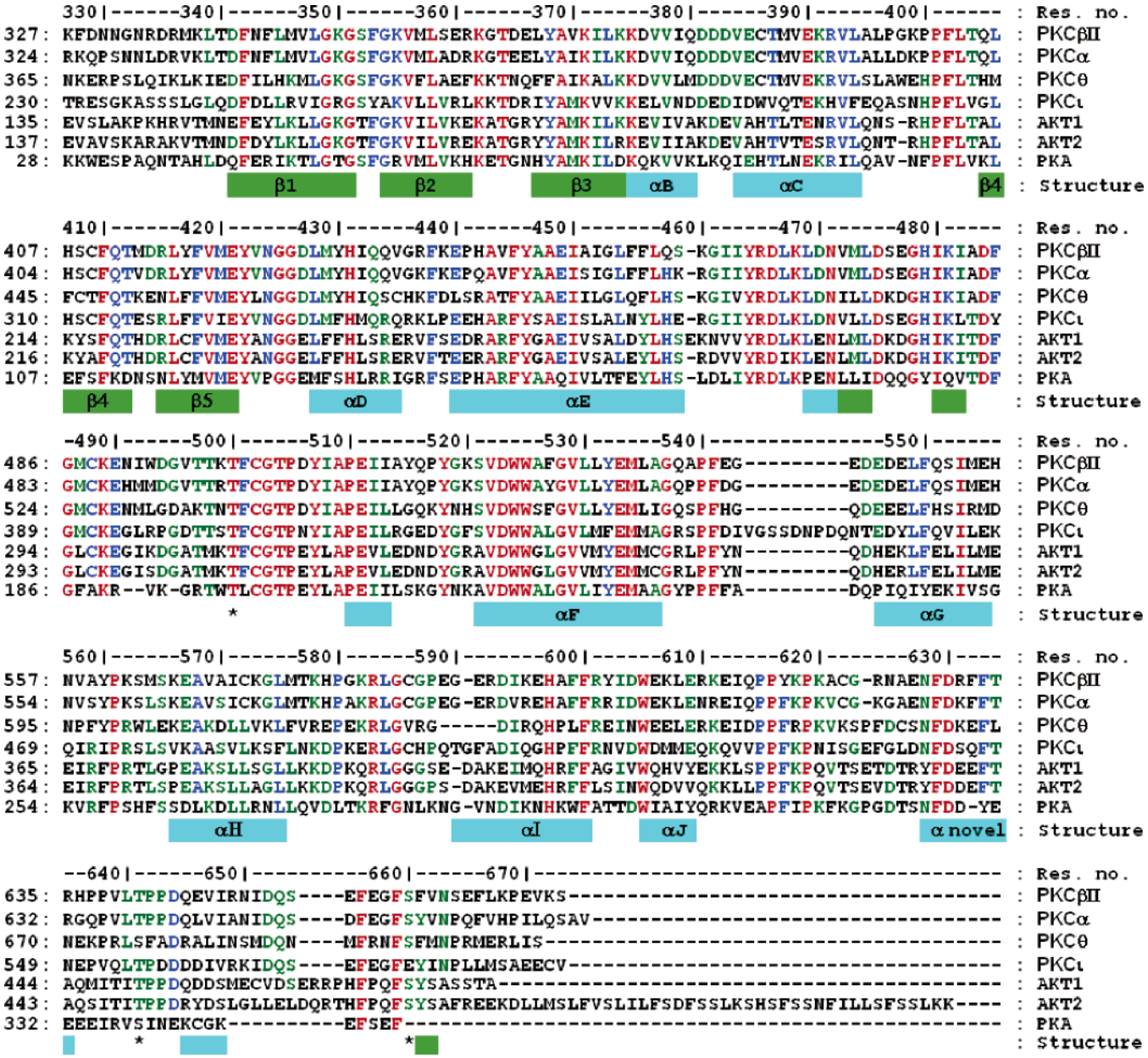

FIGURE 3: Alignment of kinase domain amino acid sequences for selected human AGC kinases. Invariant (identical) residues across all seven kinases are shown in red, and nonconserved residues are shown in black. Of the remaining residues, those with at least 80% similarity are in blue, and those with 60−80% similarity are in green. PKCβII residues are labeled by horizontal numbers which identify the sequence by a | symbol. Vertical numbers correspond to the starting residue in each line for the aligned kinase. T500, T641, and S660 phosphorylation sites are denoted by a * symbol. Secondary structure elements are indicated in green for β strands and cyan for α helices and identified by standard nomenclature. The novel α helix seen in the current structure is also specified.

Not previously observed in related PKC family members, this PKCβII kinase domain structure contains a novel α helix (residues 629−636) in the first part of the turn motif (of monomer A only) which associates with the N-terminal lobe, with implications for a relatively exposed ATP site (Figures 4A and 5A). The side chains of conserved residues Phe-629 and Phe-633 are spatially adjacent and lie against a nonpolar surface formed by N-lobe residues Leu-345, Met-346, Leu-358, and Leu-367, along with main chain atoms of Arg-624 (Figure 5B). While this helix is remote from the ATP site entrance, in its current position it could play a role in stabilizing residues that comprise the active site, e.g., strand β1 of the glycine-rich loop. In the crystal there are additional interactions between this helix and that of a symmetry-related molecule (denoted here monomer A′), resulting in a clustering of phenyl side chains from Phe-629, Phe-632, and Phe-633 contributed by each molecule (Figure 5B). There is also a water-mediated hydrogen bond between the inhibitor of monomer A and His-636′ ND of monomer A′; however, His-636 of monomer A is too far from the inhibitor for any intramolecular interaction. Because crystal packing may contribute to the conformation and position of the turn helix, its functional role for the enzyme remains difficult to assess from this crystal structure. However, the same general position for this helix was observed in another cocrystal structure of PKCβII recently determined in our laboratory (data not shown) which involved completely different crystal packing. The average temperature factor for atoms in the turn region of PKCβII is 70 Å^2, relative to a core average value of 51 Å^2, suggesting a significant degree of flexibility

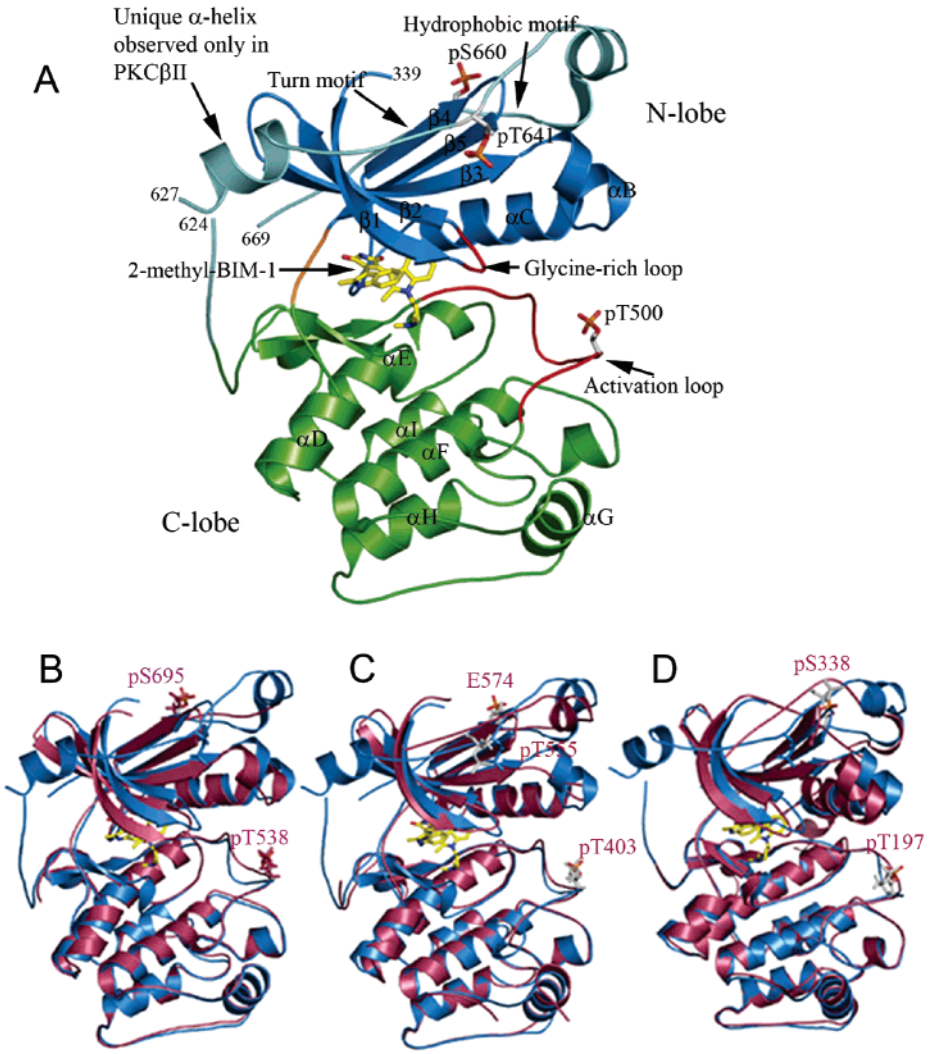

FIGURE 4: Overall structure of the PKCβII−2-methyl-1*H*-indol-3-yl-BIM-1 complex and comparison with selected AGC kinases. (A) Ribbon representation of the PKCβII catalytic domain structure. The N-lobe is in sky blue, the C-lobe is in green, the hinge region is in orange, and the C-terminal region is in cyan. The glycine-rich loop and activation loop are highlighted in red. 2-Methyl-1*H*-indol-3-yl-BIM-1 and phosphorylated residues are shown in stick representations. In this orientation, helix αE is partially blocked by helix αD. (B) Superposition of PKCβII−2-methyl-1*H*-indol-3-yl-BIM-1 (sky blue ribbon; 2-methyl-1*H*-indol-3-yl-BIM-1 and phosphorylated residues are shown in stick representations) and PKCθ−staurosporine [raspberry ribbons and sticks; PDB code 1XJD (*32*)]. (C) Superposition of PKCβII−2-methyl-1*H*-indol-3-yl-BIM-1 [color coding as described for (B)] and PKCι−BIM-1 [raspberry ribbons and sticks; PDB code 1ZRZ (*33*)]. (D) Superposition of PKCβII−2-methyl-1*H*-indol-3-yl-BIM-1 [color coding is the same as described for (B)] and PKA−Bim2molA structures [raspberry ribbons and sticks; PDB code 1SZM (*48*)]. Phosphorylated sites in PKAα, PKCθ, and PKCι are also shown.

and potential readjustment; therefore, some degree of interaction between the turn helix and active site ligands cannot be excluded for PKCβII in solution.

Comparison with Other Relevant AGC Kinases. Kinases are often classified into three conformational states: closed, intermediate, and open, as measured by the disposition of the N-lobe relative to the C-lobe (*49*). The crystal structure of PKCβII−2-methyl-1*H*-indol-3-yl-BIM-1 has been superimposed on the structures of PKCθ−staurosporine (1XJD) (*32*), PKCι−BIM1 (1ZRZ) (*33*), and PKA−Bim2 (PDB code 1SZM) (*48*), as shown in Figure 4B−D, respectively. These aligned structures display good agreement in their overall conformations. Comparative analysis of these PKC−inhibitor structures indicates that the current PKCβII structure represents an "intermediate" conformation with respect to ATP-competitive inhibitor binding. A similar intermediate conformation was also observed for PKA and other PKC isoform cocrystal structures with a bound BIM analogue (Figure 4B−D) (*32*, *33*, *48*). For these kinases, the measured distances between the catalytic Lys-371 and Glu-390 of helix αC (or equivalent residues of the structures shown in Figure 4B−D) are 2.6−2.9 Å, suggesting that a salt bridge is still present in all of the structures. However, there are no hydrogen bonds formed between the tip of helix αC and the activation loop of PKCβII, which is also indicative of a kinase in an intermediate conformation.

In most intermediate kinase structures, the glycine-rich phosphate-binding loop connecting strands β1 and β2 (GxGxxG) also adopts a position that is intermediate between open and closed positions (*50*, *51*), and this the case for PKCβII residues 349−355. The open and closed positions can be defined by measuring the distance between the glycine-rich loop and the activation loop. In PKCβII, the distance from Ser-352:CA on the glycine-rich loop to Gly-486:CA on the activation loop is 8.7 Å, similar to the PKA structure with BIM-2 for molecule A (denoted here PKA−

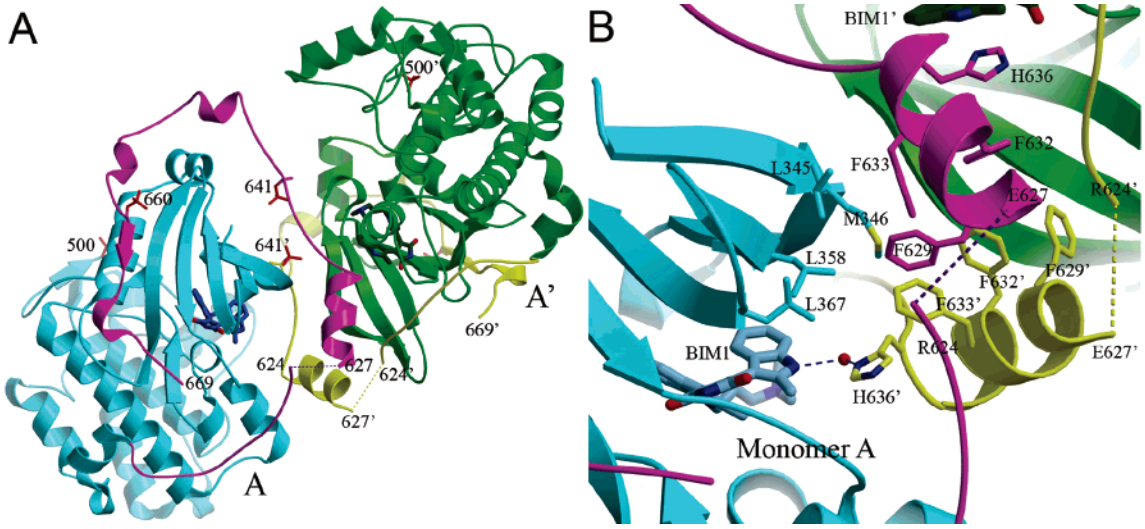

FIGURE 5: C-Terminus of PKCβII in the crystal. (A) Two molecules of monomer A related by crystallographic symmetry, denoted A (cyan core with magenta C-terminus) and A′ (green core with yellow C-terminus), showing mutual intermolecular association of the turn region α helices (629−636). (B) Closeup of the interface between monomers A and A′. Conserved residues Phe-629 and Phe-633 (magenta) pack against a hydrophobic patch on monomer A (cyan) but also participate in the cluster of phenylalanine side chains that includes Phe-623 and the three equivalent residues from monomer A′. The water-mediated hydrogen bond between the inhibitor of monomer A and His-636′ is likely specific to this crystal form.

Bim2molA) where the equivalent distance is 9.8 Å (Figure 6A). However, for PKCθ (*32*) with the more planar staurosporine-bound inhibitor, the serine to glycine distance is only 5.5 Å, representing a closed conformation. At the other extreme, the recently reported structure for PKCι with BIM-1 (*33*) contains an open glycine-rich loop conformation, with a Ser-255 to Gly-389 distance of 13.5 Å, in spite of the overall enzyme displaying an intermediate state. This may result from the fact that PKCι has a tyrosine residue (PKCβII position 353) in place of the conserved phenylalanine seen in the other PKCs and PKA. The larger size and polarity of tyrosine may also explain the lower inhibition activity of BIM-1 against PKCι compared to other PKC isoforms (Table 3). Additionally, in the PKCβII structure, Phe-353 is flipped inward toward the inhibitor while pointed away from Lys-371, in a manner similar to the PKA−Bim2molA crystal structure. In contrast, the glycine-rich loop of the PKCθ−staurosporine structure (*32*) lies deep inside the phosphate binding site, forcing Phe-391 (equivalent to PKCβII Phe-353) to orient toward Lys-409 (Lys-371 in PKCβII), thus shielding the phosphate binding site and restricting access to residues critical for catalysis, possibly explaining the greater inhibition of PKCθ by staurosporine relative to other AGC kinases.

Conformation of the Bound Inhibitor. In the current structure, 2-methyl-1*H*-indol-3-yl-BIM-1 binds to PKCβII in a manner similar to that of the previously reported cocrystal structures for PKA−BIM2molA and PKCι−BIM1 (*33*, *48*). The inhibitor is bound in a cleft between the two lobes, in the ATP-binding site of both molecules. These ATP-competitive inhibitors form four hydrogen bonds with the protein and several van der Waals interactions with residues from the N- and C-lobes and the hinge linker region (Figure 6B). The maleimide ring makes two hydrogen bonds to the backbone of the hinge region: from nitrogen to Glu-421:O (2.9 Å) and from a carbonyl oxygen to Val-423:N (3.1 Å). Two other hydrogen bonds are formed from the other maleimide carbonyl oxygen, one to the side chain of Thr-404:OG1 (2.9 Å) and the other to HOH-60 (3.4 Å). A fourth hydrogen bond with the protein is found between the nitrogen of the dimethylamino group and OD1 of Asp-470 (2.8 Å) on the catalytic loop. One of the indole rings of 2-methyl-1*H*-indol-3-yl-BIM-1 is flipped in a manner similar to that found in other AGC kinase family members complexed with BIM-1 (*33*, *48*). This may account for the nonselectivity of the indolocarbazole-containing inhibitors toward PKC isoforms. It further appears that most BIM analogues make a similar set of hydrogen-bonding contacts with AGC kinases. This inhibitor conformation is not possible with indolocarbazole-containing PKC inhibitors like staurosporine because of the planarity of the ring system. Inhibitor selectivity might therefore be derived from hydrophobic interactions, or from utilization of minor structural features that are unique to each PKC isoform, rather than from hydrogen bond disruptions. However, no obvious structural features are apparent within this PKCβII−inhibitor complex when compared with other AGC−BIM binary structures to account for the selective affinity of this compound for PKCβII.

The macrocyclic, bisindolylmaleimide ruboxistaurin has been reported to be a potent and highly selective inhibitor of PKCβII. Recently, this clinical candidate was cocrystallized with PDK1, the upstream kinase for phosphorylation of some PKC ioforms (*46*). In an attempt to better understand the nature of the PKCβII selectivity profile of ruboxistaurin, the binding of inhibitor into the PKCβII kinase domain structure was modeled. Although a single binding mode was observed in the PDK1−inhibitor complex (*46*), modeling of the compound with PKCβII gave the unexpected result that two binding modes are possible. One of the binding modes produced a conformation for the inhibitor that is similar to that observed in the reported PDK1 complex. A second binding mode for the inhibitor was also determined from the docking model. In this second docking model, the inhibitor was flipped 180 degrees as compared to the first conformation, orienting the dimethylamine side chain more toward solvent. Of the two binding models, the docking procedure employed here indicated that the second, flipped conformation of the inhibitor was more energetically favor-

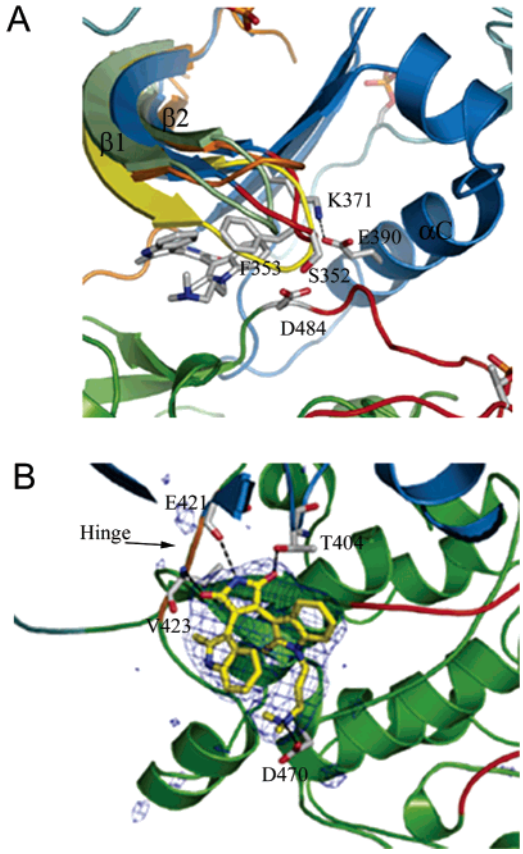

FIGURE 6: Glycine-rich loop inhibitory arrangement and 2-methyl-1*H*-indol-3-yl-BIM-1 binding site with electron density map. (A) Glycine-rich loop of 2-methyl-1*H*-indol-3-yl-BIM-1 bound PKCβII (highlighted in red) in comparison with the glycine-rich loops of the PKA−Bim2molA structure [in pale green, PDB code 1SZM (*48*)], the PKCθ−staurosporine structure [in yellow, PDB code 1XJD (*32*)], and the PKCι−BIM-1 [in orange, PDB code 1ZRZ (*33*)]. Hydrogen bonding in the phosphate recognition site is depicted by black dashed lines. (B) 2-Methyl-1*H*-indol-3-yl-BIM-1 (in sticks) bound to the ATP-binding pocket of PKCβII (ribbon representation) with the corresponding $|F_o - F_c|$ electron density, derived from the phases of the protein only, contoured in blue at 3.0σ. Hydrogen bond interactions between inhibitor atoms and enzyme residues (sticks) are depicted by black dashed lines.

able. While unexpected, there is a structural precedent for this dual binding mode for bisindolylmaleimides, where BIM-2 was reported to adopt two distinct binding modes in the PKA cocrystal structure (*48*).

Activation Loop and αC *Helix*. For protein kinases, the activation loop and the αC helix play important roles in catalysis. The activation loop provides part of the binding surface for peptide and protein substrates and, together with the αC helix, serves as a docking site for cofactors (*51*). In most protein kinases, these structural regions fold into an active conformation as a consequence of phosphorylation (*49*). The activation loop observed in the PKCβII kinase structure is phosphorylated and is in an extended conformation (Figure 7). The phosphate on Thr-500 forms an ion pair with Arg-465 of the catalytic loop and Lys-489 of the activation loop. This orients the catalytic base, Asp-466, for catalysis and Glu-490 for hydrogen bonding to Arg-392 of the αC helix. In turn, this rearrangement orients the helix αC such that Glu-390 may hydrogen bond with catalytic Lys-371, aligning helix αC into a position for substrate binding. In addition, pThr-500 also hydrogen bonds to the side chain of Thr-498, further stabilizing the activation loop. Additionally, Glu-385 forms another salt bridge with Arg-392 on helix αC, further anchoring helix αC to the activation loop. While this network is similar to that seen in other PKC isoforms, there is a notable difference in PKA. The phosphate of the equivalent activation loop Thr-197 (PKA numbering) can form a hydrogen bond with His-87 at the tip of helix αC, orienting helix αC into a closed conformation. In novel and conventional PKCs, the equivalent residue is a cysteine (residue 386 in PKCβII) and tryptophan in atypical PKCs. Therefore, Cys-386 may be required for substrate binding in novel and conventional PKCs. All PKCs contain an additional single residue insertion at the end of αC helix that shortens the αC−β4 loop, making it less flexible and rather unique relative to other AGC family members. PKCθ has a bulky tryptophan in this position whereas other PKCs have a small serine residue, making PKCθ unique in that the tryptophan shapes and stabilizes the surface on which its own hydrophobic motif segment docks (*32*).

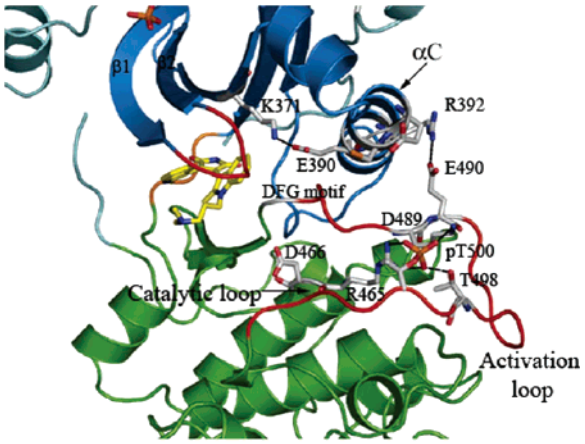

FIGURE 7: The activation loop and helix αC. Ribbon drawing of PKCβII (N-lobe is in sky blue, C-lobe is in green) highlighting key structural motifs at the active site, with the activation loop shown in red. Selected residues are in stick representation. Dashed black lines depict specific hydrogen-bonding interactions of the essential pThr-500 phosphate with the cationic pocket (Arg-465, Lys-489) and of helix αC with the catalytic Lys-371 and the activation loop (Glu-490).

*Phosphorylation Sites in Turn and Hydrophobic Motif*s. The C-terminal hydrophobic motif is phosphorylated at Ser-660 in this PKCβII structure, a requirement for optimal enzyme activity. The structural role of this phosphorylation site appears to be a tightening of the N-lobe to help to align helix αC for catalysis (*52*, *53*). The three aromatic side chains of the hydrophobic motif, Phe-656, Phe-659, and Phe-661, form lipophilic interactions with helices αB and αC, and strands β4 and β5, as shown in Figure 8A. There are also several hydrogen bonds anchoring the hydrophobic motif to helix αC and strand β4. For example, the backbone of Phe-659 is hydrogen bonded to the side chain of Lys-391 of helix αC, while the phosphate of Ser-660 is hydrogen bonded to the conserved Gln-411 on strand β4. Similar interactions are observed in the PKCθ−staurosporine and PKCι−BIM-1 protein crystal structures, where a glutamate residue (a phosphate mimic) is present and serves the same role. In contrast, PKA has a hydrophobic motif that terminates at Phe-350 (Phe-659 in PKCβII) and therefore lacks a site for regulatory phosphorylation. Alternatively, the C-terminal carboxylate of PKA may play a similar stabilization role as the hydrophobic phospho-Ser in PKCβII.

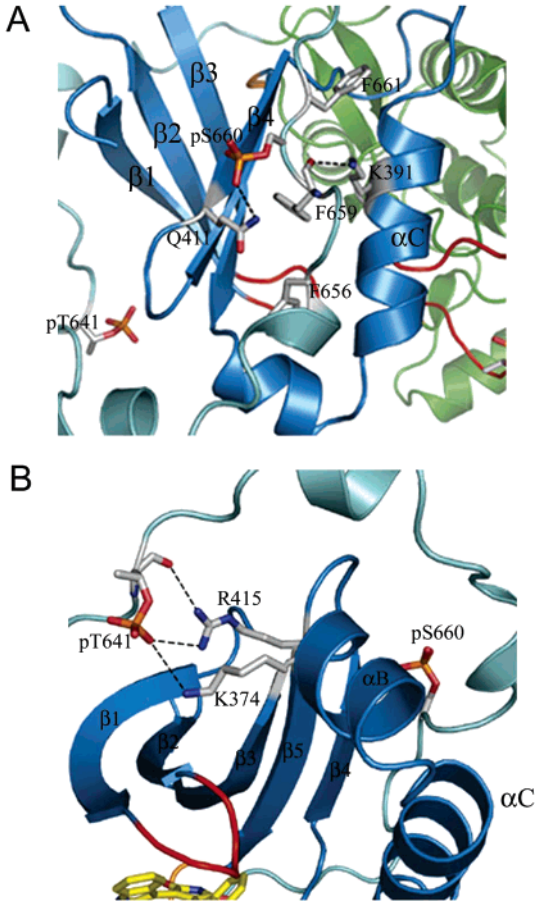

FIGURE 8: The hydrophobic and turn motif phosphorylation sites. Ribbons of the N-lobe are in sky blue, the C-lobe is in green, and the C-terminus portion is in cyan. (A) Hydrophobic motif phosphorylation site of PKCβII. Hydrogen-bonding contacts formed by pSer-660, backbone atoms of the hydrophobic motif, and residues in the N-lobe (sticks) are indicated by dashed black lines. (B) Turn motif phosphorylation site of PKCβII. Hydrogen-bonding contacts formed by pThr-641 and residues in the N-lobe (sticks) are indicated by dashed black lines.

The turn motif of AGC kinases exhibits a phosphorylation site (either phospho-Ser or phospho-Thr) at position 641 (PKCβII numbering). In the PKA−BIM2molA and PKCι−BIM-1 structures, the corresponding serine residue is phosphorylated and anchors the C-terminus at the top of the N-lobe. It has been reported that, for PKAα and PKCβII, mutation of the residue at this position may destabilize the kinase domain, generate an inactive kinase, and/or cause precipitation of the protein. This suggests that phosphorylation of this turn motif serine or threonine is important in stabilizing the catalytic domain by associating the C-terminus with the N-lobe (*54*, *55*). The turn motif phosphorylation site was not observed in the crystal structure of PKCθ, although the active enzyme is known to be phosphorylated at that site. In the PKCβII structure, the turn motif phosphorylation site is well-defined in molecule A. The phosphate group on Thr-641 forms ionic contacts with Lys-374 from strand β3 and Arg-415 from strand β5 (Figure 8B), similar to those reported for the PKCι−BIM-1 structure. In the PKAα structure, the phosphate of Ser-338 makes contacts with adjacent residues on the turn motif and therefore has a different arrangement from that observed in PKCβII and PKCι. The novel PKC ioforms, PKCθ and PKCδ, have an asparagine or histidine, respectively, in place of Arg-415, possibly explaining why the turn−motif is not well-defined in the PKCθ−staurosporine structure (*32*).

In summary, the structure of the PKCβII catalytic domain complexed with BIM-1 reveals several interesting features not observed previously with other PKC−isoform kinase domain structures. These include the observation of a fully phosphorylated kinase domain, the presence of a unique α helix at the C-terminus, and the adoption of an intermediate overall conformation that lies in between the typical open and closed forms. Given the diverse roles of conventional PKC isoforms and their high sequence homology, this structure for the PKCβII catalytic domain provides a tool for the further design of potent inhibitors.

ACKNOWLEDGMENT

We acknowledge the assistance of Keira Maiden and Ciaran Cronin for evaluation of PKCβII kinase domain expression in bacterial and insect cell systems. We thank Michael Gehring and Marc Deller for helpful suggestions for expression and crystallization of the kinase. We also thank Michael Jirousek and Michael Niesman for encouragement and advice. We acknowledge that portions of this research were conducted at the Advanced Light Source, a national user facility operated by Lawrence Berkeley National Laboratory, on behalf of the U.S. Department of Energy, Office of Basic Energy Sciences. The Berkeley Center for Structural Biology is supported in part by the Department of Energy, Office of Biological and Environmental Research, and by the National Institutes of Health, National Institute of General Medical Sciences.

REFERENCES

1. Nishizuka, Y. (1992) Membrane phospholipid degradation and protein kinase C for cell signalling, *Neurosci Res. 15*, 3−5.
2. Newton, A. C. (2004) Diacylglycerol's affair with protein kinase C turns 25, *Trends Pharmacol. Sci. 25*, 175−177.
3. Hofmann, J. (1997) The potential for isoenzyme-selective modulation of protein kinase C, *FASEB J. 11*, 649−669.
4. Kanashiro, C. A., and Khalil, R. A. (1998) Signal transduction by protein kinase C in mammalian cells, *Clin. Exp. Pharmacol. Physiol. 25*, 974−985.
5. Liu, W. S., and Heckman, C. A. (1998) The sevenfold way of PKC regulation, *Cell. Signalling 10*, 529−542.
6. Mellor, H., and Parker, P. J. (1998) The extended protein kinase C superfamily, *Biochem. J. 332* (Part 2), 281−292.
7. Newton, A. C. (1997) Regulation of protein kinase C, *Curr. Opin. Cell Biol. 9*, 161−167.
8. Way, K. J., Katai, N., and King, G. L. (2001) Protein kinase C and the development of diabetic vascular complications, *Diabetic Med. 18*, 945−959.
9. Koya, D., and King, G. L. (1998) Protein kinase C activation and the development of diabetic complications, *Diabetes 47*, 859−866.
10. Inoguchi, T., Battan, R., Handler, E., Sportsman, J. R., Heath, W., and King, G. L. (1992) Preferential elevation of protein kinase C isoform beta II and diacylglycerol levels in the aorta and heart of diabetic rats: differential reversibility to glycemic control by islet cell transplantation, *Proc. Natl. Acad. Sci. U.S.A. 89*, 11059−11063.
11. Shiba, T., Inoguchi, T., Sportsman, J. R., Heath, W. F., Bursell, S., and King, G. L. (1993) Correlation of diacylglycerol level and protein kinase C activity in rat retina to retinal circulation, *Am. J. Physiol. 265*, E783−E793.
12. Wu, L. W., Mayo, L. D., Dunbar, J. D., Kessler, K. M., Baerwald, M. R., Jaffe, E. A., Wang, D., Warren, R. S., and Donner, D. B. (2000) Utilization of distinct signaling pathways by receptors for vascular endothelial cell growth factor and other mitogens in the induction of endothelial cell proliferation, *J. Biol. Chem. 275*, 5096−5103.
13. Xia, P., Aiello, L. P., Ishii, H., Jiang, Z. Y., Park, D. J., Robinson, G. S., Takagi, H., Newsome, W. P., Jirousek, M. R., and King,

G. L. (1996) Characterization of vascular endothelial growth factor's effect on the activation of protein kinase C, its isoforms, and endothelial cell growth, *J. Clin. Invest. 98*, 2018−2026.
14. Takahashi, T., Ueno, H., and Shibuya, M. (1999) VEGF activates protein kinase C-dependent, but Ras-independent Raf-MEK-MAP kinase pathway for DNA synthesis in primary endothelial cells, *Oncogene 18*, 2221−2230.
15. Suzuma, K., Takahara, N., Suzuma, I., Isshiki, K., Ueki, K., Leitges, M., Aiello, L. P., and King, G. L. (2002) Characterization of protein kinase C beta isoform's action on retinoblastoma protein phosphorylation, vascular endothelial growth factor-induced endothelial cell proliferation, and retinal neovascularization, *Proc. Natl. Acad. Sci. U.S.A. 99*, 721−726.
16. Ishii, H., Jirousek, M. R., Koya, D., Takagi, C., Xia, P., Clermont, A., Bursell, S. E., Kern, T. S., Ballas, L. M., Heath, W. F., Stramm, L. E., Feener, E. P., and King, G. L. (1996) Amelioration of vascular dysfunctions in diabetic rats by an oral PKC beta inhibitor, *Science 272*, 728−731.
17. Joy, S. V., Scates, A. C., Bearelly, S., Dar, M., Taulien, C. A., Goebel, J. A., and Cooney, M. J. (2005) Ruboxistaurin, a protein kinase C {beta} inhibitor, as an emerging treatment for diabetes microvascular complications, *Ann. Pharmacother*. (in press).
18. Group, T. P.-D. S. (2005) The effect of ruboxistaurin on visual loss in patients with moderately severe to very severe nonproliferative diabetic retinopathy: initial results of the protein kinase c beta inhibitor diabetic retinopathy study (PKC-DRS) multicenter randomized clinical trial, *Diabetes 54*, 2188−2197.
19. Strom, C., Sander, B., Klemp, K., Aiello, L. P., Lund-Andersen, H., and Larsen, M. (2005) Effect of ruboxistaurin on blood-retinal barrier permeability in relation to severity of leakage in diabetic macular edema, *Invest. Ophthalmol. Visual Sci. 46*, 3855−3858.
20. Tuttle, K. R., Bakris, G. L., Toto, R. D., McGill, J. B., Hu, K., and Anderson, P. W. (2005) The effect of ruboxistaurin on nephropathy in type 2 diabetes, *Diabetes Care 28*, 2686−2690.
21. Newton, A. C. (1993) Interaction of proteins with lipid headgroups: lessons from protein kinase C, *Annu. Rev. Biophys. Biomol. Struct. 22*, 1−25.
22. Bell, R. M., and Burns, D. J. (1991) Lipid activation of protein kinase C, *J. Biol. Chem. 266*, 4661−4664.
23. Newton, A. C. (1995) Protein kinase C. Seeing two domains, *Curr. Biol. 5*, 973−976.
24. Keranen, L. M., Dutil, E. M., and Newton, A. C. (1995) Protein kinase C is regulated in vivo by three functionally distinct phosphorylations, *Curr. Biol. 5*, 1394−1403.
25. Tsutakawa, S. E., Medzihradszky, K. F., Flint, A. J., Burlingame, A. L., and Koshland, D. E., Jr. (1995) Determination of in vivo phosphorylation sites in protein kinase C, *J. Biol. Chem. 270*, 26807−26812.
26. Dutil, E. M., Toker, A., and Newton, A. C. (1998) Regulation of conventional protein kinase C isozymes by phosphoinositide-dependent kinase 1 (PDK-1), *Curr. Biol. 8*, 1366−1375.
27. Behn-Krappa, A., and Newton, A. C. (1999) The hydrophobic phosphorylation motif of conventional protein kinase C is regulated by autophosphorylation, *Curr. Biol. 9*, 728−737.
28. Zhang, G., Kazanietz, M. G., Blumberg, P. M., and Hurley, J. H. (1995) Crystal structure of the cys2 activator-binding domain of protein kinase C delta in complex with phorbol ester, *Cell 81*, 917−924.
29. Verdaguer, N., Corbalan-Garcia, S., Ochoa, W. F., Fita, I., and Gomez-Fernandez, J. C. (1999) Ca(2+) bridges the C2 membrane-binding domain of protein kinase Calpha directly to phosphatidylserine, *EMBO J. 18*, 6329−6338.
30. Sutton, R. B., and Sprang, S. R. (1998) Structure of the protein kinase Cbeta phospholipid-binding C2 domain complexed with Ca^{2+}, *Structure 6*, 1395−1405.
31. Pappa, H., Murray-Rust, J., Dekker: L. V., Parker, P. J., and McDonald, N. Q. (1998) Crystal structure of the C2 domain from protein kinase C-delta, *Structure 6*, 885−894.
32. Xu, Z. B., Chaudhary, D., Olland, S., Wolfrom, S., Czerwinski, R., Malakian, K., Lin, L., Stahl, M. L., Joseph-McCarthy, D., Benander, C., Fitz, L., Greco, R., Somers, W. S., and Mosyak, L. (2004) Catalytic domain crystal structure of protein kinase C-theta (PKCtheta), *J. Biol. Chem. 279*, 50401−50409.
33. Messerschmidt, A., Macieira, S., Velarde, M., Badeker, M., Benda, C., Jestel, A., Brandstetter, H., Neuefeind, T., and Blaesse, M. (2005) Crystal structure of the catalytic domain of human atypical protein kinase C-iota reveals interaction mode of phosphorylation site in turn motif, *J. Mol. Biol. 352*, 918−931.
34. Parker, G. J., Law, T. L., Lenoch, F. J., and Bolger, R. E. (2000) Development of high throughput screening assays using fluorescence polarization: nuclear receptor-ligand-binding and kinase/phosphatase assays, *J. Biomol. Screening 5*, 77−88.
35. Cook, P. F., Neville, M. E., Jr., Vrana, K. E., Hartl, F. T., and Roskoski, R., Jr. (1982) Adenosine cyclic 3′,5′-monophosphate dependent protein kinase: kinetic mechanism for the bovine skeletal muscle catalytic subunit, *Biochemistry 21*, 5794−5799.
36. Zhao, Z. H., Malencik, D. A., and Anderson, S. R. (1991) Characterization of a new substrate for protein kinase C: assay by continuous fluorometric monitoring and high performance liquid chromatography, *Biochem. Biophys. Res. Commun. 176*, 1454−1461.
37. Morrison, J. F. (1969) Kinetics of the reversible inhibition of enzyme-catalysed reactions by tight-binding inhibitors, *Biochim. Biophys. Acta 185*, 269−286.
38. Otwinowski, Z., and Minor, W. (1997) Processing X-ray diffraction data collected in oscillation mode, in *Methods in Enzymology* (Carter, C. W., Jr., and Sweet, R. M., Eds.) pp 307−326, Academic Press, New York.
39. Navaza, J. (1994) AMoRe: an automated package for molecular replacement, *Acta Crystallogr. A 50*, 157−163.
40. Murshudov, G. N., Vagin, A. A., and Dodson, E. J. (1997) Refinement of macromolecular structures by the maximum-likelihood method, *Acta Crystallogr., Sect. D: Biol. Crystallogr. 53*, 240−255.
41. McRee, D. E. (1992) XtalView: a visual protein crystallographic system for X11/Xview, *J. Mol. Graphics 10*, 44−47.
42. Laskowski, R. J., MacArthur, M. W., Moss, D. S., and Thornton, J. M. (1993) PROCHECK: a program to check the stereochemical quality of protein structures, *J. Appl. Crystallogr. 26*, 283−291.
43. DeLano, W. L. (2002) PyMOL (Scientific, D., Ed.), Publisher, San Carlos, CA.
44. Gehlhaar, D. K., Verkhivker, G. M., Rejto, P. A., Sherman, C. J., Fogel, D. B., Fogel, L. J., and Freer, S. T. (1995) Molecular recognition of the inhibitor AG-1343 by HIV-1 protease: conformationally flexible docking by evolutionary programming, *Chem. Biol. 2*, 317−324.
45. Bouzida, D., Gehlhaar, D. K., Rejto, P. A. (1998) *Proc. Eur. Symp. Q. Struct. Relat., 12th QSAR Symp., 2000*, 425−426.
46. Komander, D., Kular, G. S., Schuttelkopf, A. W., Deak, M., Prakash, K. R., Bain, J., Elliott, M., Garrido-Franco, M., Kozikowski, A. P., Alessi, D. R., and van Aalten, D. M. (2004) Interactions of LY333531 and other bisindolyl maleimide inhibitors with PDK1, *Structure (Cambridge) 12*, 215−226.
47. Goekjian, P. G., and Jirousek, M. R. (1999) Protein kinase C in the treatment of disease: signal transduction pathways, inhibitors, and agents in development, *Curr. Med. Chem. 6*, 877−903.
48. Gassel, M., Breitenlechner, C. B., Konig, N., Huber, R., Engh, R. A., and Bossemeyer, D. (2004) The protein kinase C inhibitor bisindolyl maleimide 2 binds with reversed orientations to different conformations of protein kinase A, *J. Biol. Chem. 279*, 23679−23690.
49. Huse, M., and Kuriyan, J. (2002) The conformational plasticity of protein kinases, *Cell 109*, 275−282.
50. Johnson, L. N., Noble, M. E., and Owen, D. J. (1996) Active and inactive protein kinases: structural basis for regulation, *Cell 85*, 149−158.
51. Johnson, D. A., Akamine, P., Radzio-Andzelm, E., Madhusudan, M., and Taylor, S. S. (2001) Dynamics of cAMP-dependent protein kinase, *Chem. Rev. 101*, 2243−2270.
52. Yang, J., Cron, P., Good, V. M., Thompson, V., Hemmings, B. A., and Barford, D. (2002) Crystal structure of an activated Akt/protein kinase B ternary complex with GSK3-peptide and AMP-PNP, *Nat. Struct. Biol. 9*, 940−944.
53. Yang, J., Cron, P., Thompson, V., Good, V. M., Hess, D., Hemmings, B. A., and Barford, D. (2002) Molecular mechanism for the regulation of protein kinase B/Akt by hydrophobic motif phosphorylation, *Mol. Cell 9*, 1227−1240.
54. Yonemoto, W., McGlone, M. L., Grant, B., and Taylor, S. S. (1997) Autophosphorylation of the catalytic subunit of cAMP-dependent protein kinase in *Escherichia coli*, *Protein Eng. 10*, 915−925.
55. Edwards, A. S., Faux, M. C., Scott, J. D., and Newton, A. C. (1999) Carboxyl-terminal phosphorylation regulates the function and subcellular localization of protein kinase C betaII, *J. Biol. Chem. 274*, 6461−6468.

BI061128H